Published in final edited form as:
Acta Biomater. 2015 January 15; 12: 195–206. doi:10.1016/j.actbio.2014.10.033.

The effects of glycosaminoglycan degradation on the mechanical behavior of the posterior porcine sclera

Barbara J. Murienne[a,*], **Joan L. Jefferys**[b], **Harry A. Quigley**[b], and **Thao D. Nguyen**[a]

Barbara J. Murienne: bmurien1@jhu.edu

[a]Department of Mechanical Engineering, Johns Hopkins University, Baltimore, MD, USA

[b]Glaucoma Center of Excellence, Johns Hopkins University School of Medicine, Baltimore, MD, USA

Abstract

Pathological changes in scleral glycosaminoglycan (GAG) content and in scleral mechanical properties have been observed in eyes with glaucoma and myopia. The purpose of this study is to investigate the effect of GAG removal on the scleral mechanical properties to better understand the impact of GAG content variations in the pathophysiology of glaucoma and myopia. We measured how the removal of sulphated GAG (s-GAG) affected the hydration, thickness and mechanical properties of the posterior sclera in enucleated eyes of 6–9 month-old pigs. Measurements were made in 4 regions centered on the optic nerve head (ONH) and evaluated under 3 conditions: no treatment (control), after treatment in buffer solution alone, and after treatment in buffer containing chondroitinase ABC (ChABC) to remove s-GAGs. The specimens were mechanically tested by pressure-controlled inflation with full-field deformation mapping using digital image correlation (DIC). The mechanical outcomes described the tissue tensile and viscoelastic behavior. Treatment with buffer alone increased the hydration of the posterior sclera compared to controls, while s-GAG removal caused a further increase in hydration compared to buffer-treated scleras. Buffer-treatment significantly changed the scleral mechanical behavior compared to the control condition, in a manner consistent with an increase in hydration. Specifically, buffer-treatment led to an increase in low-pressure stiffness, hysteresis, and creep rate, and a decrease in high-pressure stiffness. ChABC-treatment on buffer-treated scleras had opposite mechanical effects than buffer-treatment on controls, leading to a decrease in low-pressure stiffness, hysteresis, and creep rate, and an increase in high-pressure stiffness and transition strain. Furthermore, s-GAG digestion dramatically reduced the differences in the mechanical behavior among the 4 quadrants surrounding the ONH as well as the differences between the circumferential and meridional responses compared to the buffer-treated condition. These findings demonstrate a significant effect of s-GAGs on both the stiffness and time-dependent behavior of the sclera. Alterations in s-GAG content may contribute to the altered creep and stiffness of the sclera of myopic and glaucoma eyes.

[*]Corresponding author at: The Johns Hopkins University, Department of Mechanical Engineering, Latrobe Hall 200, 3400 N. Charles St., Baltimore, MD 21218, USA, Tel.: +1 410 516 8781, fax: +1 410 516 7254.

Conflict of interest: None.

Keywords

Sclera; Glaucoma; Myopia; Chondroitinase ABC; Inflation

1. Introduction

The sclera, the white outer shell of the eye, is responsible for maintaining the eye shape in the presence of intraocular pressure and protecting the internal ocular structures from external forces. It is the main load-bearing tissue of the eye and studies have suggested that alterations to its mechanical properties, specifically at the posterior pole, contribute to the development of glaucoma and myopia [1]. Glaucoma is the second leading cause of blindness worldwide [2] and glaucoma damage is considered to be dependent on the scleral mechanical properties [3–5]. Myopia is a common refractive error that is ubiquitous in certain populations [6] and the associated abnormal axial elongation of the globe involves dramatic changes in the scleral mechanical properties [7].

Changes in the extracellular matrix (ECM) structure of the eye wall have been reported with both glaucoma and myopia. These include variations in the GAG content. GAGs are polysaccharide chains of various lengths, the majority of which bind to core proteins to form proteoglycans (PGs). The human posterior sclera is particularly rich in chondroitin sulfate GAG side chains [8], from the abundant presence of aggrecan [9], and in dermatan sulfate chains [8]. An abnormal accumulation of GAGs, including chondroitin sulfates, was reported in some portions of the anterior segment [10] and in the ONH [11] of glaucomatous human eyes. Similarly, the rat ONH [12] and monkey lamina cribrosa [13] showed a higher chondroitin sulfate content when subjected to IOP elevation. A decrease in GAG content was found in the posterior sclera of human myopic eyes [14] and tree-shrews with form-deprivation myopia [15]. A decrease in GAG synthesis was also reported in the posterior sclera of form-deprived myopic tree shrew [16] and monkey eyes [17].

Changes in the tensile and viscoelastic properties of the sclera also occur in glaucoma and myopia. The posterior sclera of glaucoma eyes showed an increase in stiffness [18–20] and a decrease in creep rate [20]. Myopic posterior scleras, in which there is a decrease in GAG content, had the opposite biomechanical changes in some parameters, with an increase in tissue extensibility [14,21,22] and creep rate [22,23] and no change in stiffness [21,23].

GAGs play an important role in the structure and mechanical behavior of collagenous ECM tissues. GAGs fill the space between the collagen fibrils and the collagen–elastin network in the ECM. Although the core protein of some PGs is found at regular intervals on collagen fibrils [24–26], it seems that PG interactions with collagen not only occur through binding of the core protein [27], but also through electrostatic interaction [28] of the GAGs themselves as shown *in vitro* [28–31]. The majority of GAGs attract water and are highly polar, due to their negatively charged carboxyl and sulphated groups. Their fixed charge density also creates attraction/repulsion forces among themselves and with collagen fibrils. As a result, the GAG content helps to determine the tissue hydration [32] by determining the number of polar sites for water binding and the space for free water uptake [33], as well as the tissue swelling pressure [34–36], which is highly dependent on hydration [37]. Hydration is

believed to regulate the spacing between collagen fibrils in the ECM [38,39]. GAGs have been shown to regulate collagen fibrillogenesis *in vitro* under certain conditions, specifically affecting the rate of fibril formation [40–42] and fibril diameter [43,44].

The mechanical functions of GAGs have been studied in various tissues, with tissue-specific and sometimes conflicting results, by comparing their mechanical behavior before and after GAG removal. In cartilage, GAG removal produced a faster creep rate [45]. This led the authors of the study to speculate that GAGs may have a role in the damping function of cartilage by providing friction and viscous resistance to interfibrillar sliding. In aortic heart valve leaflets, where native creep is negligible, no change in the creep behavior was observed after GAG removal [46]. GAG removal does not change the hysteresis observed during cyclic loading in ligaments [47] nor at the high stress range in heart valve leaflets [46]. In contrast, it decreased the hysteresis in aortic valve leaflets in the low stress range [46]. A faster relaxation was observed after GAG removal in the aorta [48], but no changes in relaxation were observed in ligaments [49]. The role of GAGs in the tissue stiffness is still controversial. No change in the uniaxial loading stiffness was found after GAG removal in cartilage [45] and tendons [50]. However, an increase in stiffness occurred in mesenteric arteries [51] and lungs [52]. In the aorta, the small-strain stiffness was higher and the high-strain stiffness lower after GAG removal, and similar changes were measured for incubation in buffer with or without a GAG-targeting enzyme compared to controls [48]. Similarly, ligaments showed a higher small-strain stiffness after GAG depletion [53], whereas no change in stiffness was measured in another study [47].

None of the studies comparing the biochemical and biomechanical characteristics of normal and pathological sclera have addressed the mechanical function of GAGs. In this study, we investigated the effect of s-GAG removal on the mechanical behavior of the posterior sclera to infer the mechanical relevance of pathological changes in scleral s-GAG content.

2. Methods

This section describes the methods used to evaluate the mechanical behavior and structural characteristics of the porcine posterior sclera.

2.1. Experimental design and glycosaminoglycan removal

All mechanical and structural outcomes were measured in 4 quadrants of the posterior scleral cup surrounding the ONH (superior–temporal (ST), superior–nasal (SN), inferior–temporal (IT), inferior–nasal (IN)). Different specimens were used for either hydration measurement (n = 18) or s-GAG quantification (n = 18) and they were divided into 3 experimental groups. In the first group, the specimens were processed immediately after preparation (control) (n = 6). In the second group, they were incubated for 18 h at 37 °C in a modified Trizma buffer at pH 8.0 (buffer-treated) (n = 6). In the third group, they were incubated for 18 h in Trizma buffer containing ChABC (C2905, Sigma–Aldrich, St. Louis MO) at 2 units/ml (enzyme-treated) (n = 6).

Other specimens used for both mechanical testing and thickness measurement (n = 12) were divided into 2 groups only. In one group, the specimens were mechanically tested after

dissection and again after incubation in buffer alone for 18 h (protocol 1: control/buffer-treated) (n = 5). In another group, the specimens were soaked in buffer alone for 18 h after dissection, mechanically tested, soaked in enzyme solution for 18 h, and tested again (protocol 2: buffer-treated/enzyme-treated) (n = 7). Thickness data for 3 additional control/buffer-treated specimens and 2 additional buffer-treated/enzyme-treated specimens that were not inflation tested were added for statistical analysis. After incubation, the samples were always rinsed for 30 min in fresh Trizma buffer without enzyme. Table 1 summarizes the number of specimens used in each experiment.

The control specimens represented a baseline hydrated state in that the interior surface of the specimens was exposed to Dulbecco's Phosphate Buffered Saline (DPBS) during the inflation test and the specimens were tested in a humidity chamber at greater than 90% humidity. Comparing controls to specimens soaked in buffer alone allowed the effect of an increase in hydration on the scleral mechanical properties to be measured. The comparison between the control (baseline hydrated) and buffer-treated (swollen) states allowed the effect of hydration to be distinguished from that of s-GAG degradation when the specimens were treated with buffer containing ChABC.

2.2. Specimen preparation

Eyes from 6–9 month-old pigs (Animal Technologies Inc., Tyler TX) were received on wet ice 24 h after enucleation and used upon arrival. The skin, extraocular fat and muscles were first carefully removed from all eyes using fine dissection scissors to obtain a clean scleral surface. The eyes used for either mechanical testing and thickness measurement or s-GAG quantification were mounted on a custom-made acrylic holder, using a cyanoacrylate-based glue (Permabond 910, Electron Microscopy Sciences, Hatfield PA). The specimens were positioned such that the posterior scleral cup protruded through the holder opening centered about the ONH (Fig. 1(a)). After the glue polymerized, a cut was made through the cornea using a scalpel and the intraocular structures including the retina and choroid were removed with fine curved dissecting forceps, leaving only the scleral shell. The remaining anterior sclera was then scored through its thickness and glued to the back side of the holder. The eyes used for hydration measurement were prepared using an 8 mm biopsy punch to extract scleral discs 2 mm away from the ONH in each of the 4 quadrants (Fig. 2). Care was taken not to include the ciliary arteries or other apparent vessels in these punch specimens. The scleral shells and discs were either processed directly or first incubated in solution, depending on their experimental group.

2.3. Hydration measurement

Scleral hydration was defined as the wet over dry tissue weight ratio. To measure the wet weight, the 8 mm scleral discs (Fig. 2) were blotted dry on a Whatman filter for 1 min, transferred to pre-weighed Eppendorf centrifuge tubes to prevent evaporation and weighed on a precision balance (XP26DR, Mettler-Toledo LLC, Columbus OH). The dry weight was obtained in the same way after the samples were dried for 48 h in an oven at 60 °C.

2.4. Glycosaminoglycan quantification

s-GAG quantification was performed on 3 × 4 mm scleral rectangles, dissected from the scleral cups 2 mm away from the ONH, in each of the 4 anatomical quadrants (Fig. 2), using the Bio-color Blyscan assay (Accurate Chemical & Scientific Corporation, Westbury NY). Prior to the assay, the samples were weighed wet after being blotted dry on Whatman paper for 1 min and then completely digested using Papain (P3125, Sigma–Aldrich, St. Louis MO) in an oven at 60 °C, following the protocol used by Boubriak et al. [54]. The s-GAG content was reported in μg/mg dry tissue weight by inferring the dry weight from the wet weight using the hydration data for the corresponding experimental group and quadrant.

2.5. Mechanical testing

For mechanical testing, the scleral shells were placed on a pressure chamber and secured though the holder (Fig. 1(c) and (d)). A series of pressure-controlled inflation tests was conducted at room temperature by injection of DPBS inside the pressure chamber using an MTS-actuated syringe (MTS, Eden Prairie MN). The testing protocol was implemented in TestWorks (MTS, Eden Prairie MN) which used pressure readings from a pressure transducer (TJE, 2 psig range, Honeywell, Morristown NJ) for PID control of the MTS. The specimens were equilibrated at baseline pressure 0.28 kPa for 30 min. Then, they were subjected to a load–unload cycle from baseline to 6 kPa at 0.13 kPa/s, a 30 min recovery period at baseline, a ramp-hold cycle loaded at 1 kPa/s to 6 kPa and held for 20 min, a 40 min recovery period at baseline, and finally a load–unload cycle identical to the first one. The specimens were encapsulated in a clear perspex hydration chamber filled with water saturated humidifier filters (Fig. 1(c) and (d)), that guaranteed a humidity level above 90% throughout the duration of the tests.

2.6. Thickness measurement

The thickness was measured at the baseline pressure, at the end of each mechanical test series. Eight different locations, at equal distance from the ONH and acrylic holder (Fig. 2), were measured using an ultrasound transducer with frequency 15 MHz (V260-45, Olympus NDT Inc., Waltham MA), fitted with a Sonopen tip with diameter 1.5 mm (DLP-302, Olympus NDT Inc., Waltham MA) and connected to a pulser–receiver (5073PR-15-U, Olympus NDT Inc., Waltham MA). The ultrasound echoes generated by the external and internal scleral walls were acquired on an oscilloscope (TDS220, Tektronix Inc., Beaverton OR) and the peak-to-peak time difference Δt between the echoes was calculated using a custom-written Matlab code. From the peak-to-peak time difference Δt and assuming a speed of sound in the sclera c_{sclera} = 1597 m/s [55], the thickness T was calculated as follows:

$$T=\frac{1}{2}c_{sclera}\Delta t \quad (1)$$

The thickness was reported as the average of 2 measurements acquired for each quadrant.

2.7. Digital Image Correlation

A stereovision system (Fig. 1(c) and (d)) composed of two monochrome cameras (GRAS-20S4M-C, Point Grey, Richmond BC, Canada) with 2 Mpixel resolution, a 24° stereo angle, 1× objectives with a 35 mm focal length (Xenoplan 1.9/35 mm-0901, Schneider Optics, Hauppauge NY) and controlled by Vic-Snap 2009 (Correlated Solutions Inc., Columbia SC) was used to acquire images of the scleral surface every 2 s during mechanical testing. The sclera was speckled with black India ink (Fig. 1(b)) using an airbrush (ECL4500 HP-CS, Iwata Medea Inc., Portland OR) to allow for 3-dimensional DIC using Vic3D 2009 (Correlated Solutions Inc., Columbia SC).

2.8. Strain calculation

DIC provided positions (X, Y, Z) of the specimen surface at the baseline pressure and displacements (U, V, W) at each pressure step for points of a Cartesian ($\mathbf{e}_x$,$\mathbf{e}_y$) grid, with grid spacing 0.12 mm on average. To calculate the circumferential and meridional strains on the surface (Fig. 1 (b)), we fit the (X, Y, Z) positions of the reference surface, for the region starting 1 mm away from the ONH, to a generalized sphere and created a curvilinear grid on the surface of the sphere ($\mathbf{e}_\theta$,$\mathbf{e}_\phi$), with grid spacing 3° in the circumferential $\mathbf{e}_\theta$ direction and 1° in the meridional $\mathbf{e}_\phi$ direction. The average geometric residual of the sphere fit for all specimens ranged between 0.0048% and 0.014% of the radius of the sphere. The 3D displacements of the DIC Cartesian grid at each pressure step were interpolated to points on the spherical grid using the Matlab function TriScatteredInterp. The stretches, $\lambda_{\theta\theta}$ in the circumferential direction and $\lambda_{\phi\phi}$ in the meridional direction, were calculated from the deformed lengths l_θ and l_ϕ and undeformed lengths L_θ and L_ϕ of material grid lines along the circumferential and meridional directions as follows [56]:

$$\lambda_{\theta\theta}=\frac{l_\theta}{L_\theta};\lambda_{\phi\phi}=\frac{l_\phi}{L_\phi} \quad (2)$$

For a point n at position θ on the undeformed spherical grid, surrounded by points $n-1$ ($\theta-\Delta\theta$) and $n+1$ ($\theta+\Delta\theta$) along the $\mathbf{e}_\theta$ direction, L_{θ_n} and l_{θ_n} were calculated using central difference as:

$$L_{\theta_n}=\sqrt{(X_{n+1}-X_{n-1})^2+(Y_{n+1}-Y_{n-1})^2+(Z_{n+1}-Z_{n-1})^2} \quad (3a)$$

$$l_{\theta_n}=\sqrt{(x_{n+1}-x_{n-1})^2+(y_{n+1}-y_{n-1})^2+(z_{n+1}-z_{n-1})^2}, \quad (3b)$$

where $x = X + U$, $y = Y + V$, $z = Z + W$. The l_{ϕ_n} and L_{ϕ_n} were similarly calculated for the $\mathbf{e}_\phi$ direction. The corresponding Lagrangian strains $E_{\theta\theta}$ and $E_{\phi\phi}$ were calculated as:

$$E_{\theta\theta}=\frac{1}{2}(\lambda_{\theta\theta}^2-1);E_{\phi\phi}=\frac{1}{2}(\lambda_{\phi\phi}^2-1) \quad (4)$$

The strains were reported in each quadrant as an average over a region spanning 90° in the circumferential direction, 12° in the meridional direction. This corresponded on average to a 3 mm wide region spanning each quadrant located 3 mm away from the ONH (Fig. 2).

2.9. Hoop stress calculation

The hoop stresses, $\sigma_{\theta\theta}$ in the circumferential direction and $\sigma_{\phi\phi}$ in the meridional direction, were approximated using the thin shell theory. For all specimens the ratio of thickness to radius satisfied $T/r < 0.1$. For a spherical thin shell, the hoop stresses are:

$$\sigma_{\theta\theta}=\sigma_{\phi\phi}=\frac{Pr}{2T}. \quad (5)$$

The stresses were calculated for the 4 quadrants at each level of pressure P, based on the radius r and the thickness T obtained for each specimen from the spherical fit of the strain calculation and the thickness measured in each quadrant, respectively.

2.10. Mechanical data analysis

Six mechanical outcomes were defined (Fig. 3) to compare the tensile and viscoelastic behavior between the quadrants and experimental groups. The slope of the stress–strain loading curves at low and high pressures, and the transition strain at the onset of strain-stiffening were calculated to characterize the stiffness and non-linearity of the tensile response. The low-pressure slope was determined by fitting a line to the data points with strains below 2/3 of the maximum strain. The high-pressure slope was evaluated by fitting a line to the last 30% of the total number of data points. The intersection between the low and high pressure lines defined the transition strain. The hysteresis of the load–unload stress–strain curves and the normalized creep rate of the ramp-hold strain–time curves were calculated to characterize the viscoelastic response. The hysteresis, defined as the area between the load– unload curves, was calculated by numerical integration using the trapezoidal rule. The initial creep rate of the first 80 s and the final creep rate of the final 1120 s were calculated from the strain–time curves. The creep rate was defined as the slope of the linear fit of the strain–time response, normalized by the strain at the end of the loading curve and plotted on a log time scale.

2.11. Statistical analysis

For hydration and s-GAG quantification data, generalized estimating equation models were used to account for repeat measurements taken in the 4 quadrants of a single specimen. For the thickness data, linear mixed models were used to consider both the clustering of 2 experimental groups within each specimen (control/buffer-treated groups or buffer-treated/enzyme-treated groups) and the repeat measurements in the 4 quadrants for each group. For each outcome, the variogram and Akaike's Information Criteria were used to determine whether measurements from adjacent quadrants were more highly correlated than measurements from opposing quadrants (Toeplitz structure) or measurements from any 2 quadrants were similarly correlated (compound symmetry structure). For all models, a Bonferroni adjustment allowed for multiple comparisons. A significant interaction between quadrant and group indicated that the group effect depended on the quadrant studied and that

the quadrant effect depended on the group studied. When the interaction was not significant, the models were simplified to combine all groups when looking at the quadrants and all quadrants when looking at the groups. For the mechanical data, paired Student's t-tests were used to compare the control and buffer-treated groups, as well as the buffer-treated and enzyme-treated groups. They were also used to compare the circumferential and meridional responses. Unpaired t-tests allowed for control to enzyme-treated comparisons. Linear mixed models were used to look at the spatial variation of the mechanical outcomes among quadrants. A p-value equal or less than 0.055 was considered significant. All analyses were performed using the Matlab Statistical Toolbox and SAS 9.2 (SAS Institute, Cary, NC).

3. Results

3.1. Glycosaminoglycan content, hydration and thickness

3.1.1. Glycosaminoglycan content—The scleral s-GAG content was obtained for the 3 experimental groups and 4 quadrants (Table 2). The statistical analysis showed a significant interaction between group and quadrant ($p < 0.0001$). The s-GAG content was not significantly different between control and buffer-treated groups in all quadrants, but enzyme-treatment decreased the s-GAG content by 79.7% on average compared to controls and by 81.5% on average compared to buffer-treated specimens ($p < 0.0001$). In the control group, the s-GAG content significantly differed by quadrant ($p < 0.005$), being on average 68.2% higher in the superior quadrants than the inferior quadrants. Similarly, in the buffer-treated group, the s-GAG content in the 2 superior quadrants was on average 71.6% higher than in the 2 inferior quadrants ($p < 0.0001$). In the enzyme-treated group, only the SN quadrant was significantly different from the inferior quadrants ($p \leq 0.01$). Its s-GAG content was 24.4% lower on average than in the inferior quadrants and not higher, as measured in the control and buffer-treated groups.

3.1.2. Hydration—The scleral hydration, defined as the wet/dry weight ratio, was obtained for the 3 experimental groups and 4 quadrants (Table 3). No significant interaction was found between group and quadrant ($p = 0.17$). Hydration was 6.8% higher in buffer-treated than controls ($p = 0.001$) and 6.0% greater in enzyme-treated than buffer-treated ($p < 0.005$). It was 13.3% higher in enzyme-treated compared to controls ($p < 0.0001$). Hydration was the same in all quadrants except for SN where it was on average 2.8% higher ($p < 0.05$).

3.1.3. Thickness—The scleral thickness was measured for the 4 quadrants and the buffer-treated data from both groups 1 and 2 repeat measurements were combined to reflect the 3 conditions: control, buffer-treated and enzyme-treated (Table 4). No significant interaction was found between group and quadrant ($p = 0.43$). The thickness was 8.3% larger in buffer-treated than controls ($p < 0.0001$) and 2.1% larger in enzyme-treated than buffer-treated ($p = 0.01$). It was 10.6% greater in enzyme-treated than controls ($p < 0.0001$). In all groups, the superotemporal sclera was thickest and the inferonasal was thinnest ($p < 0.0001$). On average, the thickness was 26.4% higher in the superior quadrants than inferior quadrants.

3.2. Mechanical behavior

3.2.1. Comparing the experimental groups—We first compared average data for all scleral regions for each of the 6 mechanical outcomes between the 2 inflation test sessions in each of the 2 protocols: control condition compared to buffer-treated (Table 5), and buffer-treated compared to enzyme-treated (Table 6). In the circumferential direction, for protocol 1, treatment in buffer alone increased the low-pressure stiffness by 28.4% ($p < 0.005$), hysteresis by 16.7% ($p < 0.01$), initial creep rate by 45.1% ($p < 0.005$), and final creep rate by 42.7% ($p < 0.05$) compared to the baseline control values. In addition, buffer-treatment decreased the high-pressure stiffness by 22.3% ($p< 0.0001$) over controls, but there was no significant change in the transition strain. In protocol 2, treatment in enzyme led to a significant decrease in the low-pressure stiffness by 51.5% ($p< 0.0001$) and hysteresis by 24.9% ($p < 0.0001$) compared to the values after treatment in buffer alone. Moreover, enzyme-treatment increased the high-pressure stiffness by 23.0% ($p < 0.05$) and the transition strain by 25.7% ($p = 0.001$) over buffer-treated specimens but there was no difference in the creep rates.

In the meridional direction, for protocol 1, buffer-treatment increased the low-pressure stiffness by 32.8% ($p < 0.05$), hysteresis by 20.8% ($p < 0.05$), and final creep rate by 288.2% ($p < 0.005$) compared to control values. Buffer-treatment also decreased the high-pressure stiffness by 27.6% ($p < 0.005$) over controls but there was no significant change in the transition strain or the initial creep rate. Compared to the effect seen with buffer-treatment in protocol 1, enzyme-treatment in protocol 2 led to nearly the opposite effects with decreased low-pressure stiffness (−54.5%, $p < 0.0005$), hysteresis (−31.2%, $p< 0.0001$), initial creep rate (−57.5%, $p < 0.001$), and final creep rate (−42.9%, $p = 0.055$), as well as increased high-pressure stiffness (+55.4%, $p< 0.0005$) and transition strain (+36.5%, $p < 0.0005$) over buffer-treated specimens.

We then compared the data between controls and enzyme-treated specimens (Table 7), though this comparison must take into account that the enzyme-treatment was performed on eyes that had undergone buffer-treatment first. Compared to controls, enzyme-treated specimens showed a significantly lower low-pressure stiffness in the circumferential (−62.3%, $p< 0.0001$) and meridional (−61.7%, $p< 0.005$) directions. They also had a lower high-pressure stiffness circumferentially (−30.7%, $p< 0.0005$) and higher final creep rate meridionally (+163.9%, $p < 0.05$). In addition, the transition strain was significantly higher in enzyme-treated than controls in the circumferential (+71.0%, $p< 0.0001$) and meridional (+111.5%, $p < 0.001$) directions.

Fig. 4 shows the average stress–strain and strain–time curves for the 3 experimental groups, for the IN quadrant, in the circumferential direction. The curves for the buffer-treated group were generated with the specimens from protocol 1.

3.2.2. Comparing the circumferential and meridional directions—We also examined the 6 mechanical outcomes for significant differences between the circumferential and meridional directions within each of the 3 conditions, control, buffer-treated and enzyme-treated (Table 8). Buffer-treated specimens from protocols 1 and 2 were combined for this analysis. In the control condition, the meridional low-pressure stiffness was 92.0%

higher than the circumferential ($p < 0.005$), while the meridional transition strain was 21.4% lower than the circumferential ($p < 0.05$). No significant differences by direction were found for the other mechanical outcomes among controls. The buffer-treated group was similar to the controls in the differences observed, also having a higher low-pressure stiffness (+100.2%, $p < 0.0001$) and lower transition strain (−9.2%, $p = 0.054$) meridionally. In addition, the high-pressure stiffness was 24.2% lower ($p < 0.0001$), initial creep rate 56.2% higher ($p<0.05$) and final creep rate 79.4% higher ($p = 0.001$) in the meridional direction compared to the circumferential direction. Interestingly, no significant differences in any mechanical outcome were found between the meridional and circumferential directions in the enzyme-treated group.

3.2.3. Group/quadrant interaction—The significance of the interaction between quadrant and experimental group for all mechanical outcomes and directions is shown in Table 9. The interaction between group and quadrant was significant for the low-pressure stiffness in the circumferential and meridional directions ($p < 0.05$), and for the transition strain ($p < 0.005$) and hysteresis ($p = 0.01$) in the meridional direction only.

3.2.4. Comparing the quadrants—To investigate spatial differences, we looked at the variability of each mechanical parameter among quadrants, in the circumferential and meridional directions (Fig. 5). For the parameters and directions with a significant interaction between group and quadrant, the results were presented for each group separately. Otherwise, all groups were combined. For the transition strain and hysteresis, the interaction between group and quadrant was not significant in the circumferential direction as opposed to the meridional direction, hence the difference in representation. The number of differences in the mechanical parameters among quadrants was higher in buffer-treated specimens than controls. However, enzyme-treated specimens showed fewer differences than those treated with buffer alone. Overall, the maximum number of differences occurred between SN/IT and ST/IN, followed by the nasal/temporal and finally the superior/inferior quadrants. The largest changes in the mechanical parameters after buffer- or enzyme-treatment were generally measured in inferior quadrants and the smallest changes in superior quadrants (data not shown here). The quadrants with the lowest and highest parameter value varied with the mechanical parameter and direction as well as group (if applicable). For all mechanical parameters, the difference between the 2 most different quadrants was always larger in the meridional direction than circumferential direction (data not presented here).

4. Discussion

To provide a better understanding of the role that s-GAGs play in the mechanical function of the sclera, we measured their content, estimated scleral hydration, thickness and measured 6 mechanical features of the scleral stress–strain and strain–time behavior before and after treatments that could affect s-GAG and scleral function.

While we found regionally greater s-GAG content in control superior sclera than inferiorly, our values are generally consistent with those of Schultz et al. [57] in the porcine posterior sclera and of Boubriak et al. [54] in the human posterior sclera. Incubation in buffer alone did not affect the s-GAG content, but treatment with ChABC reduced s-GAGs by 73–90%.

The failure to remove all s-GAGs could be caused by insufficient time for digestion, lack of penetration of enzyme into some scleral areas, or the presence of s-GAGs that are not susceptible to ChABC digestion, such as keratan sulfates.

The ratio of the wet to the dry weight of control sclera was approximately 3 to 1, with slightly higher hydration in the superior nasal region. These data are consistent with those measured in the porcine posterior sclera by Schultz et al. [57]. Buffer-treatment alone significantly increased hydration over the control values. This most likely resulted from additional water entering in the sclera, rather than a change in the other constituent molecular components. In support of this conclusion, there was no significant change in s-GAGs per dry weight. The increase in scleral thickness in buffer-treated compared to control sclera was similar in magnitude to the percent increase in hydration, again probably due to added water in the wet state of the tissue. Our control thickness results, showing a larger thickness in superior sclera than inferiorly, are comparable to those of Chen et al. [58] in the porcine posterior sclera. ChABC treatment led to an additional increase in hydration over buffer-treatment that was 13% greater than in control sclera. This is particularly interesting given the fact that the s-GAGs were largely removed by the enzyme. Furthermore, scleral thickness was only mildly increased by enzyme-treatment after buffer-treatment. This may suggest that removal of s-GAGs allowed entry of more water, but that this was accompanied by minimal volume increase, as the water occupied less volume than had the s-GAGs. A similar increase in hydration from a hydrated swollen state was observed in lungs [52] and in articular cartilage [59] after ChABC treatment and in intervertebral discs [60] after in vivo injection of ChABC. However, previous studies have shown contradictory findings on the effect of s-GAG content on hydration of the human sclera. Boubriak et al. [54] found no effect, whereas Brown et al. [32] measured a lower hydration with lower s-GAG content in the human anterior sclera. The increase in hydration after s-GAG removal can be explained by distinguishing “bound” and “free” water in a matrix composed of charged polymer chains [33]. When the polymer chains are abundant and long, which is the case of chondroitin sulfates, they tend to interact with each other creating a tight matrix. The resulting matrix has a large number of polar sites to which water binds to but not much space for free water. However, if a large majority of the polymeric chains are removed, the matrix loses water-binding sites and increases its capacity for free water absorption. This explanation is consistent with the study by Boubriak et al. [54], where a higher partition coefficient was measured after s-GAG removal in the human sclera, suggesting an increase in free space in the matrix. The effect of GAGs on hydration should vary greatly depending on the amount, type, and organization of GAGs in the tissue relative to collagen fibrils [61]. Therefore, differences between the present and Boubriak study [54] might be attributed to differences in species and incubation medium. Similarly, differences between our results and the Brown study [32] may be caused by differences in species and scleral location.

s-GAG removal had significant effects on the tensile and viscoelastic behavior of the posterior sclera. Moreover, these effects were in the opposite direction than those caused by an increase in hydration with treatment in buffer alone. For the control-buffer comparison, the faster creep rate is consistent with an increase in hydration, as observed in ligaments [62], and can be explained by the increased water content reducing friction between the collagen fibrils during deformation. Similarly, the decrease in high-pressure stiffness may be

caused by a lower interfibrillar friction with higher water content. The increase in hysteresis is likely caused by increased viscous dissipation associated to the poroelastic effect of the increased free water in the tissue. The hypothesis of an increased hydration after incubation in buffer alone is supported by the hydration and thickness data. For the buffer-enzyme comparison, the decrease in the low-pressure stiffness and increase in transition strain both point to an alteration in the crimp morphology with the removal of the s-GAGs and the connection they provide between adjacent fibrils. The slower creep rate in the meridional direction and higher high-pressure stiffness is consistent with increased interfibrillar friction with s-GAG removal. Although hydration was higher after s-GAG removal, we hypothesized that this increased water content was in the form of free water rather than that bound to s-GAGs. Free water could easily move out of the tissue during deformation, reducing the lubrication between collagen fibrils. This effect would also explain a decrease in hysteresis with the removal of s-GAGs. A similar stiffening was observed in the annulus fibrosus upon s-GAG depletion [63]. In addition, some mechanical parameters showed a significant difference between their control and enzyme-treated values. Enzyme-treated specimens had a lower low-pressure and high-pressure stiffnesses than controls. They also had higher final creep rate and transition strain. This indicates that pathological changes in scleral s-GAG content might significantly contribute to the development of an altered scleral mechanical behavior.

The effect of s-GAG removal on the mechanical properties is similar to those observed in experimental and human myopia sclera. The sclera of high myopes [14] and experimental myopia eyes [15] have a reduced s-GAG content and exhibited a more compliant load response in some studies [14,21,22]. The opposite has been observed for glaucoma, where a higher scleral stiffness has been measured [18–20]. Current studies are investigating remodeling of the collagen structure as the source of altered mechanical behavior in the sclera of glaucoma eyes. The findings of this study suggests that alterations in the GAG content may be an additional significant contributor to the altered mechanical behavior and resulting axonal damage in glaucoma eyes.

Looking at the mechanical differences between the circumferential and meridional directions, the most interesting feature was that ChABC treatment dramatically diminished the mechanical differences between the circumferential and meridional directions observed in the control and buffer-treated groups. A similar phenomenon was reported in aortic valve cusps, where the significant difference in the relaxation constant between the circumferential and radial directions disappeared after ChABC treatment [64]. Given that proteoglycans bind adjacent collagen fibrils, we can speculate that the proteoglycan arrangement is either anisotropic or enhances the anisotropy of the collagen arrangement. This points to a greater need to study the structure of proteoglycan interaction with collagen and their arrangements in the ECM.

The same phenomenon was observed when comparing the mechanical differences among the quadrants. Differences among quadrants increased with buffer-treatment from controls but decreased with enzyme-treatment from treatment in buffer alone. These observations are consistent with the result that the s-GAG content was significantly different among quadrants in the control sclera. Therefore, these regional differences in s-GAG content

induced different degrees of swelling upon incubation in buffer, thus increasing the differences in the regional mechanical behavior after treatment in buffer. Moreover, the s-GAG content became more uniform among quadrants after ChABC treatment, thus fewer differences in mechanical behavior were measured among the different quadrants. This suggests that the spatial heterogeneity of GAG organization contributes to that of the scleral mechanical behavior. More differences were measured between SN/IT and ST/IN, than between neighboring quadrants. This is consistent with the fact that the thickness and s-GAG content varied gradually from one quadrant to the other, making neighboring quadrants more similar than opposite quadrants. The largest changes in mechanical outcomes usually occurred in the inferior quadrants. This suggests that while inferior quadrants had lower s-GAG content, they were more susceptible to s-GAG removal than superior quadrants.

Limitations of this study include the absence of direct mechanical comparison between control and enzyme-treated sclera. The choice of comparing the mechanical behavior (1) before treatment (control) and after incubation in buffer alone; and (2) after incubation in buffer and after incubation in ChABC solution, was made to distinguish the effect of incubation in buffer alone, and therefore that of an increase in hydration, from that of s-GAG removal. Additional limitations include the difficulty in obtaining specimens with consistent levels of hydration because of variability in the eye collection procedure, transport, and delivery schedules from week to week. In addition, a higher DIC correlation noise was observed in scleral areas containing ciliary arteries and vortex veins, which are identified by a darker appearance. These areas are a small proportion of the sclera and their effect was minimized by averaging the strains over a whole quadrant of the sclera. The sclera is known to exhibit large local variations in strains during inflation testing [20,65,66] and averaging the strains over a large region does not allow the measurement of the effects of s-GAG removal on local variations of the mechanical behavior. The spherical thin-walled membrane model was used for the stress analysis. The model assumes a constant thickness meridionally, but the scleral thickness can vary significantly along a meridian [67]. We mitigated the effect of thickness variation in the stress analysis by considering a region only 3 mm wide meridionally, over which the variation in thickness was assumed to be small. We used ChABC C2905 from Sigma–Aldrich, which is not guaranteed to be protease-free though the contamination is low (Sigma communication). Harrisson et al. [68] showed that the proteolytic activity of the non protease-free ChABC from Sigma–Aldrich is non-detectable at low concentrations such as the one used in this study. A number of studies have used non protease-free ChABC [50,69–71] and did not find larger effects on the tissue mechanical behavior, compared to studies that used protease-free ChABC [46,51,52] or non protease-free ChABC with protease inhibitors [45,49,72]. Specifically, they showed no significant differences in the mechanical behavior upon prolonged incubation in the non protease-free enzyme. This suggests that the impurities themselves do not degrade structural components of the tissues. To confirm that the impurities present in the ChABC used in this study did not affect the mechanical outcomes, we tested a subset of eyes after incubation in buffer with inhibitors (protease inhibitor cocktail tablets S8830, Sigma–Aldrich, St. Louis MO) and after incubation in buffer with ChABC and inhibitors. The results showed the same mechanical changes as presented in the paper comparing buffer-and enzyme-treated tissues,

confirming that GAG degradation is responsible for the observed scleral mechanical changes. The DIC dynamic uncertainties, 0.05% strain in the circumferential direction and 0.07% strain the meridional direction (Appendix), were within the 0.03–0.08% strain standard deviation range reported by Sutton et al. [73]. The methodology used for uncertainty calculations can be found in the Appendix.

5. Conclusion

In conclusion, we evaluated the effects of s-GAG removal on the structure and mechanical behavior of the porcine posterior sclera and found significant differences. Our main findings were:

1. s-GAG removal increased scleral hydration.
2. s-GAG removal significantly affected both the viscoelastic and tensile behavior of the posterior sclera, in a way opposite from that of an increase in hydration.
3. s-GAG removal decreased the differences in mechanical behavior between the circumferential and meridional directions and among the **4** quadrants of the buffer-treated sclera.

In this study, s-GAGs were found to represent on average only 0.6% of the dry weight of the porcine posterior sclera. Moreover, s-GAGs are often seen as compliant molecules that do not contribute to the mechanical behavior of connective tissues. However, the results showed that s-GAGs had significant effects on the mechanical behavior of the tissue, most likely through their interaction with collagen fibrils and ability to bind water, thus preventing it from flowing through the tissue under load. The results also suggest that alterations to s-GAG content may contribute to the differences in mechanical behavior measured in glaucoma and myopia and may play an important role in the development of ocular pathologies.

Acknowledgments

This work was supported by the NIH, Grant No. EY021500.

Appendix A

Both DIC static and dynamic uncertainties were evaluated.

A.1. DIC static uncertainty

To estimate the static noise level responsible for DIC static uncertainty, a porcine scleral specimen, incubated in buffer for 18 h at 37 °C, was left to equilibrate at baseline pressure 0.28 kPa for 30 min, after which 10 consecutive pictures were rapidly taken. The corresponding strains were calculated and averaged over a 3 mm wide annulus and the 9 image sequence, using the first image as the reference. The standard deviation across the annulus and image sequence provided a measure of the DIC static uncertainty due to static noise. Results showed an average and standard deviation on displacements of − 4.2e−5 ± 1.9e−5 mm in the circumferential direction and − 7.7e−5 ± 5.5e−5 mm in the meridional

direction. Similarly, the mean and standard deviation on absolute strain, was 1.1e–5 ± 5.6e–6 in the circumferential direction and 1.4e–4 ± 9.3e–5 in the meridional direction.

A.2. DIC dynamic uncertainty

To evaluate the DIC uncertainty with inflation, a method previously described was used [56]. Briefly, a discrete spherical shell with radius 13.3 mm, corresponding to the mean radius over all specimens and tests, was created in Matlab and subjected to an inflation defined as a 195 ± 13.4 μm Gaussian distribution across its surface. The distribution mean and standard deviation values were chosen to account for DIC noise and bias on out-of-plane displacements. A bias of 195 ± 12 μm for a 200 μm applied out-of-plane displacement was reported in a previous study [20]. A noise of 1.4 μm was estimated using the mean confidence margin across the surface of one specimen, for the out-of-plane displacement at max pressure, obtained from Vic-3D. The confidence margin represents a one standard deviation taking into account initial position and displacement uncertainties due to DIC dynamic noise. The corresponding strains were computed over a 3 mm wide annulus and the standard deviation in strain across this annulus represented a measure of the DIC dynamic uncertainty due to noise and bias. Results showed an average and standard deviation of the absolute strain field of 0.0149 ± 5.2707e–4 in the circumferential direction and 0.0151 ± 6.7605e–4 in the meridional direction (Fig. 6). The mean values in both directions are close to the 0.0151 theoretical strain for a 200 μm uniform inflation and the standard deviations were small compared to the strains measured.

Appendix B. Figures with essential colour discrimination

Certain figures in this article, particularly Figure 6 are difficult to interpret in black and white. The full colour images can be found in the on-line version, at 10.1016/j.actbio.2014.10.033.

References

1. Campbell IC, Coudrillier B, Ethier CR. Biomechanics of the posterior eye: a critical role in health and disease. J Biomech Eng. 2013; 136(2):021005. [PubMed: 24356942]
2. Resnikoff S, Pascolini D, Etya'ale D, Kocur I, Pararajasegaram R, Pokharel GP, et al. Global data on visual impairment in the year 2002. Bull World Health Organ. 2004; 82(11):844–51. [PubMed: 15640920]
3. Burgoyne CF, Downs JC, Bellezza AJ, Suh JK, Hart RT. The optic nerve head as a biomechanical structure: a new paradigm for understanding the role of IOP-related stress and strain in the pathophysiology of glaucomatous optic nerve head damage. Prog Retin Eye Res. 2005; 24(1):39–73. [PubMed: 15555526]
4. Sigal IA, Flanagan JG, Tertinegg I, Ethier CR. Finite element modeling of optic nerve head biomechanics. Invest Ophthalmol Vis Sci. 2004; 45(12):4378–87. [PubMed: 15557446]
5. Sigal IA, Flanagan JG, Ethier CR. Factors influencing optic nerve head biomechanics. Invest Ophthalmol Vis Sci. 2005; 46(11):4189–99. [PubMed: 16249498]
6. Pan CW, Ramamurthy D, Saw SM. Worldwide prevalence and risk factors for myopia. Ophthalmic Physiol Optics. 2012; 32(1):3–16.
7. McBrien NA, Jobling AI, Gentle A. Biomechanics of the sclera in myopia: extracellular and cellular factors. Optomet Vis Sci. 2009; 86(1):E23–30.

8. Trier K, Olsen EB, Ammitzbll T. Regional glycosaminoglycans composition of the human sclera. Acta Ophthalmol. 1990; 68(3):304–6. [PubMed: 2392906]

9. Rada JA, Achen VR, Penugonda S, Schmidt RW, Mount BA. Proteoglycan composition in the human sclera during growth and aging. Invest Ophthalmol Vis Sci. 2000; 41(7):1639–48. [PubMed: 10845580]

10. Knepper PA, Goossens W, Hvizd M, Palmberg PF. Glycosaminoglycans of the human trabecular meshwork in primary open-angle glaucoma. Invest Ophthalmol Vis Sci. 1996; 37(7):1360–7. [PubMed: 8641839]

11. Tezel G, Edward DP, Wax MB. Serum autoantibodies to optic nerve head glycosaminoglycans in patients with glaucoma. Arch Ophthalmol. 1999; 117(7):917. [PubMed: 10408457]

12. Johnson EC, Morrison JC, Farrell S, Deppmeier L, Moore C, McGinty M. The effect of chronically elevated intraocular pressure on the rat optic nerve head extracellular matrix. Exp Eye Res. 1996; 62(6):663–74. [PubMed: 8983948]

13. Fukuchi T, Sawaguchi S, Yue BJ, Iwata K, Hara H, Kaiya T. Sulfated proteoglycans in the lamina cribrosa of normal monkey eyes and monkey eyes with laser-induced glaucoma. Exp Eye Res. 1994; 58(2):231–44. [PubMed: 8157116]

14. Avetisov E, Savitskaya N, Vinetskaya M, Iomdina E. A study of biochemical and biomechanical qualities of normal and myopic eye sclera in humans of different age groups. Metabol Pediatr Syst Ophthalmol. 1983; 7(4):183.

15. Norton TT, Rada JA. Reduced extracellular matrix in mammalian sclera with induced myopia. Vis Res. 1995; 35(9):1271–81. [PubMed: 7610587]

16. McBrien NA, Lawlor P, Gentle A. Scleral remodeling during the development of and recovery from axial myopia in the tree shrew. Invest Ophthalmol Vis Sci. 2000; 41(12):3713–9. [PubMed: 11053267]

17. Rada JA, Nickla DL, Troilo D. Decreased proteoglycan synthesis associated with form deprivation myopia in mature primate eyes. Invest Ophthalmol Vis Sci. 2000; 41(8):2050–8. [PubMed: 10892842]

18. Downs JC, Suh JF, Thomas KA, Bellezza AJ, Hart RT, Burgoyne CF. Viscoelastic material properties of the peripapillary sclera in normal and early-glaucoma monkey eyes. Invest Ophthalmol Vis Sci. 2005; 46(2):540–6. [PubMed: 15671280]

19. Girard MJ, Suh JKF, Bottlang M, Burgoyne CF, Downs JC. Biomechanical changes in the sclera of monkey eyes exposed to chronic IOP elevations. Invest Ophthalmol Vis Sci. 2011; 52(8):5656–69. [PubMed: 21519033]

20. Coudrillier B, Tian J, Alexander S, Myers KM, Quigley HA, Nguyen TD. Biomechanics of the human posterior sclera: age- and glaucoma-related changes measured using inflation testing. Invest Ophthalmol Vis Sci. 2012; 53(4):1714–28. [PubMed: 22395883]

21. Phillips J, McBrien N. Form deprivation myopia: elastic properties of sclera. Ophthal Physiol Optics. 1995; 15(5):357–62.

22. Phillips JR, Khalaj M, McBrien NA. Induced myopia associated with increased scleral creep in chick and tree shrew eyes. Invest Ophthalmol Vis Sci. 2000; 41(8):2028–34. [PubMed: 10892839]

23. Siegwart JT, Norton TT. Regulation of the mechanical properties of tree shrew sclera by the visual environment. Vis Res. 1999; 39(2):387–407. [PubMed: 10326144]

24. Scott J, Haigh M. ‘Small’-proteoglycan: collagen interactions: Keratan sulphate proteoglycan associates with rabbit corneal collagen fibrils at the ‘a’ and ‘c’ bands. Biosci Rep. 1985; 5:765–74. [PubMed: 2935202]

25. Pringle GA, Dodd CM. Immunoelectron microscopic localization of the core protein of decorin near the d and e bands of tendon collagen fibrils by use of monoclonal antibodies. J Histochem Cytochem. 1990; 38(10):1405–11. [PubMed: 1698203]

26. Fleischmajer R, Fisher LW, MacDonald ED, Jacobs L Jr, Perlish JS, Termine JD. Decorin interacts with fibrillar collagen of embryonic and adult human skin. J Struct Biol. 1991; 106(1):82–90. [PubMed: 2059554]

27. Scott JE. Proteoglycan-fibrillar collagen interactions. Biochem J. 1988; 252(2):313. [PubMed: 3046606]

28. ÖBrink B. A study of the interactions between monomeric tropocollagen and glycosaminoglycans. Eur J Biochem. 1973; 33(2):387–400. [PubMed: 4266508]
29. Hedbom E, Heinegård D. Binding of fibromodulin and decorin to separate sites on fibrillar collagens. J Biol Chem. 1993; 268(36):27307–12. [PubMed: 8262971]
30. Pogany G, Hernandez DJ, Vogel KG. The in vitro interaction of proteoglycans with type I collagen is modulated by phosphate. Arch Biochem Biophys. 1994; 313(1):102–11. [PubMed: 8053669]
31. Raspanti M, Viola M, Forlino A, Tenni R, Gruppi C, Tira ME. Glycosaminoglycans show a specific periodic interaction with type I collagen fibrils. J Struct Biol. 2008; 164(1):134–9. [PubMed: 18664384]
32. Brown C, Vural M, Johnson M, Trinkaus-Randall V. Age-related changes of scleral hydration and sulfated glycosaminoglycans. Mech Ageing Dev. 1994; 77(2):97–107. [PubMed: 7745995]
33. Bettelheim FA, Plessy B. The hydration of proteoglycans of bovine cornea. Biochim Biophys Acta (BBA)-General Subjects. 1975; 381(1):203–14.
34. Hedbys BO. The role of polysaccharides in corneal swelling. Exp Eye Res. 1961; 1(1):81–91. [PubMed: 14036117]
35. Meyer F, Silberberg A. In vitro study of the influence of some factors important for any physicochemical characterization of loose connective tissue in the microcirculation. Microvasc Res. 1974; 8(3):263–73. [PubMed: 4373638]
36. Comper WD, Laurent TC. Physiological function of connective tissue polysaccharides. Physiol Rev. 1978; 58(1):255–315. [PubMed: 414242]
37. Hedbys BO, Dohlman CH. A new method for the determination of the swelling pressure of the corneal stroma in vitro. Exp Eye Res. 1963; 2(2):122–9. [PubMed: 13963667]
38. Scott JE, Bosworth TR. A comparative biochemical and ultrastructural study of proteoglycan-collagen interactions in corneal stroma. Functional and metabolic implications. Biochem J. 1990; 270:491–7. [PubMed: 2119175]
39. Meek K, Fullwood N, Cooke P, Elliott G, Maurice D, Quantock A, et al. Synchrotron X-ray diffraction studies of the cornea, with implications for stromal hydration. Biophys J. 1991; 60(2): 467–74. [PubMed: 1912282]
40. Wood G. The formation of fibrils from collagen solutions. 3 Effect of chondroitin sulphate and some other naturally occurring polyanions on the rate of formation. Biochem J. 1960; 75(3):605. [PubMed: 13845811]
41. ÖBrink B. The influence of glycosaminoglycans on the formation of fibers from monomeric tropocollagen in vitro. Eur J Biochem. 1973; 34(1):129–37. [PubMed: 4267112]
42. Snowden JM, Swann DA. Effects of glycosaminoglycans and proteoglycan on the in vitro assembly and thermal stability of collagen fibrils. Biopolymers. 1980; 19(4):767–80.
43. Kuc I, Scott P. Increased diameters of collagen fibrils precipitated in vitro in the presence of decorin from various connective tissues. Connect Tissue Res. 1997; 36(4):287–96. [PubMed: 9610887]
44. Rühland C, Schönherr E, Robenek H, Hansen U, Iozzo RV, Bruckner P, et al. The glycosaminoglycan chain of decorin plays an important role in collagen fibril formation at the early stages of fibrillogenesis. FEBS J. 2007; 274(16):4246–55. [PubMed: 17651433]
45. Schmidt MB, Mow VC, Chun LE, Eyre DR. Effects of proteoglycan extraction on the tensile behavior of articular cartilage. J Orthop Res. 1990; 8(3):353–63. [PubMed: 2324854]
46. Eckert CE, Fan R, Mikulis B, Barron M, Carruthers CA, Friebe VM, et al. On the biomechanical role of glycosaminoglycans in the aortic heart valve leaflet. Acta Biomater. 2012; 9(1):4653–60. [PubMed: 23036945]
47. Lujan TJ, Underwood CJ, Henninger HB, Thompson BM, Weiss JA. Effect of dermatan sulfate glycosaminoglycans on the quasi-static material properties of the human medial collateral ligament. J Orthop Res. 2007; 25(7):894–903. [PubMed: 17343278]
48. Hoffman A, Grande L, Park J. Sequential enzymolysis of human aorta and resultant stress–strain behavior. Biomater Med Devices Artif Organs. 1977; 5(2):121. [PubMed: 195640]
49. Lujan TJ, Underwood CJ, Jacobs NT, Weiss JA. Contribution of glycosaminoglycans to viscoelastic tensile behavior of human ligament. J Appl Physiol. 2009; 106(2):423–31. [PubMed: 19074575]

50. Fessel G, Snedeker JG. Equivalent stiffness after glycosaminoglycan depletion in tendon – an ultra-structural finite element model and corresponding experiments. J Theor Biol. 2011; 268(1): 77–83. [PubMed: 20950629]
51. Gandley R, McLaughlin M, Koob T, Little S, McGuffee L. Contribution of chondroitin-dermatan sulfate-containing proteoglycans to the function of rat mesenteric arteries. Am J Physiol – Heart Circul Physiol. 1997; 273(2):H952–60.
52. Al Jamal R, Roughley PJ, Ludwig MS. Effect of glycosaminoglycan degradation on lung tissue viscoelasticity. Am J Physiol – Lung Cell Mol Physiol. 2001; 280(2):L306–15. [PubMed: 11159010]
53. Hoffman A, Park J, Abrahamson J. Sequential enzymolysis of ligament and resultant stress–strain behavior. Artif Cells Blood Substitutes Biotechnol. 1973; 1(3):453–67.
54. Boubriak O, Urban J, Bron A. Differential effects of aging on transport properties of anterior and posterior human sclera. Exp Eye Res. 2003; 76(6):701–13. [PubMed: 12742353]
55. Girard MJ, Downs JC, Bottlang M, Burgoyne CF, Suh JF. Peripapillary and posterior scleral mechanics, Part II–experimental and inverse finite element characterization. J Biomech Eng. 2009; 131(5):051012. [PubMed: 19388782]
56. Tonge TK, Murienne BJ, Coudrillier B, Alexander S, Rothkopf W, Nguyen TD. Minimal preconditioning effects observed for inflation tests of planar tissues. J Biomech Eng. 2013; 135(11):114502. [PubMed: 23897279]
57. Schultz DS, Lotz JC, Lee SM, Trinidad ML, Stewart JM. Structural factors that mediate scleral stiffness. Invest Ophthalmol Vis Sci. 2008; 49(10):4232–6. [PubMed: 18539943]
58. Chen K, Rowley AP, Weiland JD. Elastic properties of porcine ocular posterior soft tissues. J Biomed Mater Res Part A. 2010; 93(2):634–45.
59. Zhu W, Mow VC, Koob TJ, Eyre DR. Viscoelastic shear properties of articular cartilage and the effects of glycosidase treatments. J Orthop Res. 1993; 11(6):771–81. [PubMed: 8283321]
60. Takahashi T, Kurihara H, Nakajima Si, Kato T, Matsuzaka S, Sekiguchi T, et al. Chemonucleolytic effects of chondroitinase ABC on normal rabbit intervertebral discs: course of action up to 10 days postinjection and minimum effective dose. Spine. 1996; 21(21):2405–11. [PubMed: 8923624]
61. Muir H. Proteoglycans as organizers of the intercellular matrix. Biochem Soc Transact. 1983; 11(6):613.
62. Thornton G, Shrive N, Frank C. Altering ligament water content affects ligament pre-stress and creep behavior. J Orthop Res. 2001; 19(5):845–51. [PubMed: 11562131]
63. Nerurkar NL, Han W, Mauck RL, Elliott DM. Homologous structure–function relationships between native fibrocartilage and tissue engineered from MSC-seeded nanofibrous scaffolds. Biomaterials. 2011; 32(2):461–8. [PubMed: 20880577]
64. Borghi A, New SE, Chester AH, Taylor PM, Yacoub MH. Time-dependent mechanical properties of aortic valve cusps: effect of glycosaminoglycan depletion. Acta Biomater. 2013; 9(1):4645–52. [PubMed: 22963848]
65. Fazio MA, Grytz R, Bruno L, Girard MJ, Gardiner S, Girkin CA, et al. Regional variations in mechanical strain in the posterior human sclera. Invest Ophthalmol Vis Sci. 2012; 53(9):5326–33. [PubMed: 22700704]
66. Pyne JD, Genovese K, Casaletto L, Geest JPV. Sequential-digital image correlation for mapping human posterior sclera and optic nerve head deformation. J Biomech Eng. 2014; 136(2):021002. [PubMed: 24337344]
67. Norman RE, Flanagan JG, Rausch SM, Sigal IA, Tertinegg I, Eilaghi A, et al. Dimensions of the human sclera: thickness measurement and regional changes with axial length. Exp Eye Res. 2010; 90(2):277–84. [PubMed: 19900442]
68. Harrisson F, van Hoof J, Vanroelen C. On the presence of proteolytic activity in glycosaminoglycan-degrading enzyme preparations. J Histochem Cytochem. 1986; 34(9):1231–5. [PubMed: 3525669]
69. Rigozzi S, Müller R, Snedeker J. Local strain measurement reveals a varied regional dependence of tensile tendon mechanics on glycosaminoglycan content. J Biomech. 2009; 42(10):1547–52. [PubMed: 19394024]

70. Ventre M, Mollica F, Netti PA. The effect of composition and microstructure on the viscoelastic properties of dermis. J Biomech. 2009; 42(4):430–5. [PubMed: 19159885]

71. Miri AK, Li NY, Avazmohammadi R, Thibeault SL, Mongrain R, Mongeau L. Study of extracellular matrix in vocal fold biomechanics using a two-phase model. Biomech Model Mechanobiol. 2014:1–9. [PubMed: 23483348]

72. Fessel G, Snedeker JG. Evidence against proteoglycan mediated collagen fibril load transmission and dynamic viscoelasticity in tendon. Matrix Biol. 2009; 28(8):503–10. [PubMed: 19698786]

73. Sutton M, Ke X, Lessner S, Goldbach M, Yost M, Zhao F, et al. Strain field measurements on mouse carotid arteries using microscopic three-dimensional digital image correlation. J Biomed Mater Res Part A. 2008; 84(1):178–90.

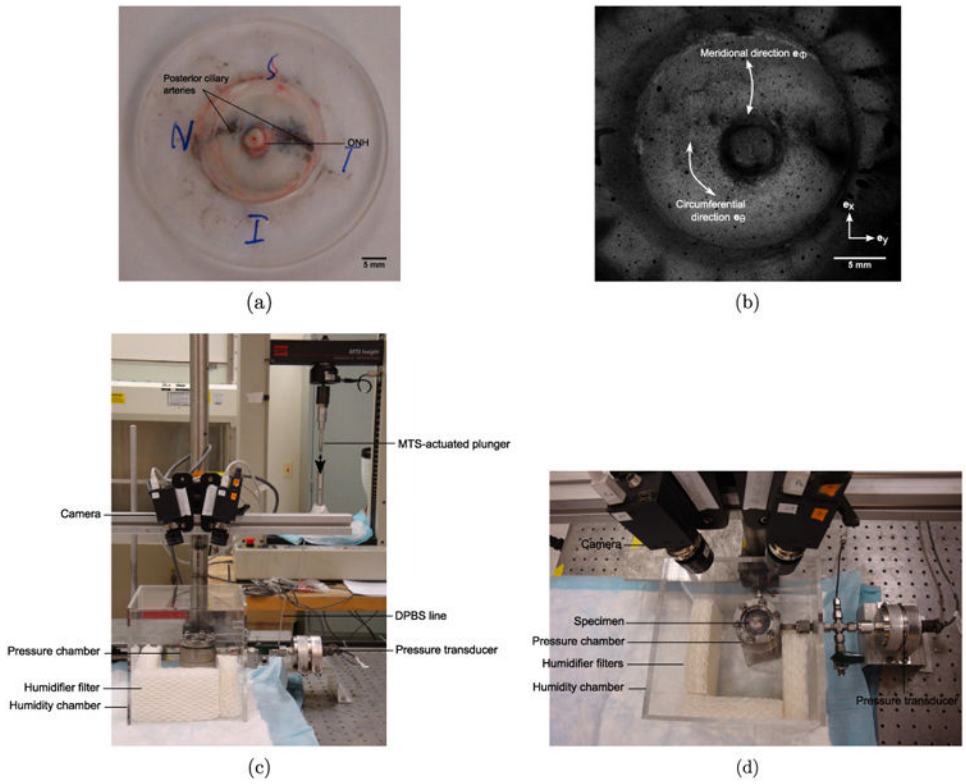

Fig. 1.

(a) Scleral shell mounted on an acrylic holder. (b) DIC image of a speckled scleral shell. Side (c) and top (d) views of the mechanical testing setup.

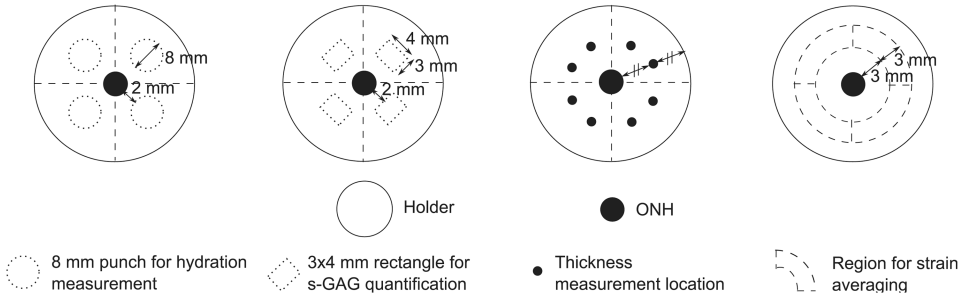

Fig. 2.

Schematic of the posterior sclera mounted on a holder showing the ONH and the locations of the 8 mm punches for hydration measurement, 3 × 4 mm rectangles for s-GAG quantification, thickness measurements and strain averaging regions.

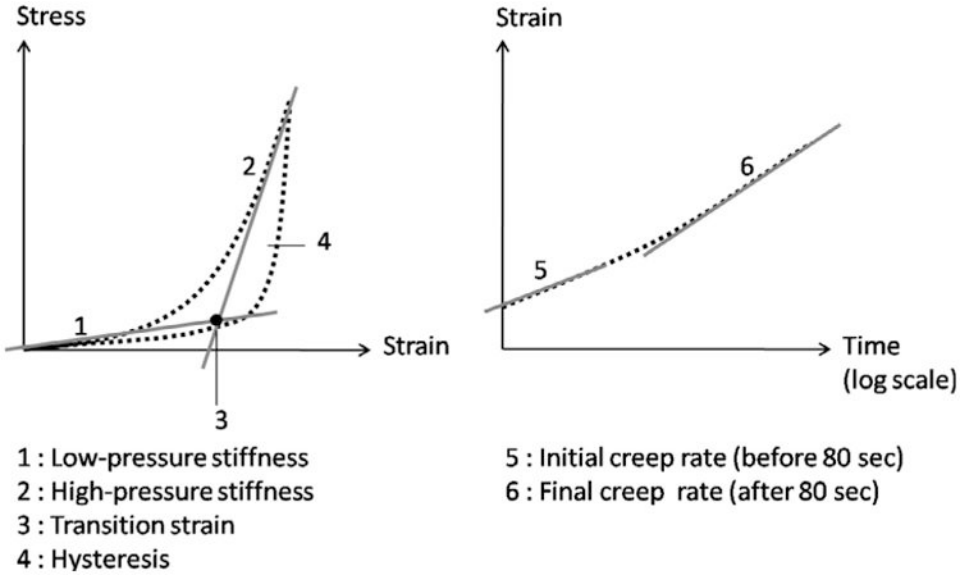

Fig. 3.

Schematic of the mechanical outcomes extracted from the load–unload stress–strain and ramp-hold strain–time curves.

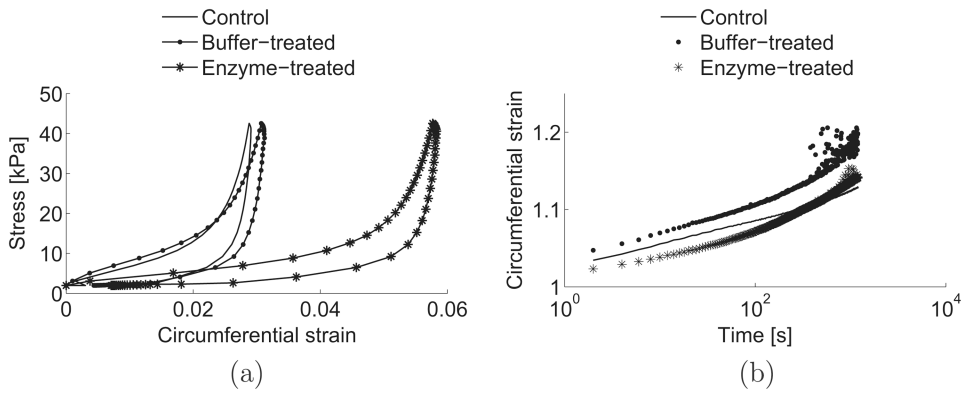

Fig. 4.

Average stress–strain (a) and strain–time (b) behaviors for the control, buffer-treated and enzyme-treated groups, for the IN quadrant, in the circumferential direction. The curves for the buffer-treated group represent the average responses of the specimens from protocol 1.

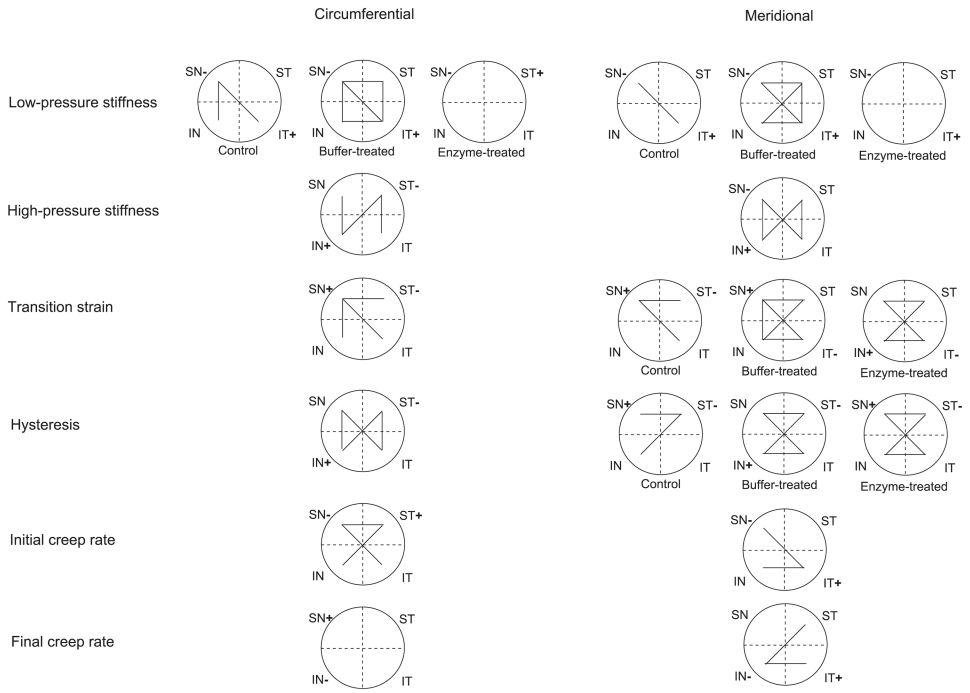

Fig. 5.

Schematic of the spatial variations for all mechanical outcomes, in the circumferential and meridional directions, assessed using linear mixed models. For the mechanical outcomes and directions having a significant interaction between group and quadrant, these variations were presented for each group. Each segment linking 2 quadrants indicates a significant difference between them. The plus and minus signs indicate the quadrants with the highest and lowest parameter value, respectively.

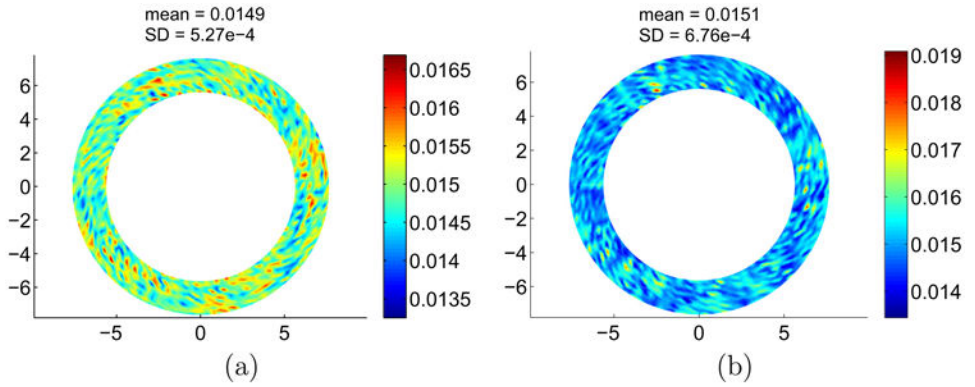

Fig. 6.

Maps of absolute circumferential (a) and meridional (b) strains, averaged over a 3 mm wide annulus, for a sphere subjected to a 195 ± 13.4 lm uniform inflation. SD = standard deviation.

Table 1

Number of specimens used for the measurement of s-GAG, hydration and changes in thickness and mechanical behavior.

	Number of specimens used for s-GAG and hydration measurements		
	Control	**Buffer-treated**	**Enzyme-treated**
s-GAG	n = 6	n = 6	n = 6
Hydration	n = 6	n = 6	n = 6
	Number of specimens used for the measurement of thickness and mechanical behavior changes		
	Control/Buffer-treated	Buffer-treated/Enzyme-treated	
Mechanical changes	n = 5	n = 7	
Thickness change	n = 8*	n = 9#	

The * denotes that 5 of the 8 specimens used to measure the thickness change were used for mechanical testing. Similarly, the # denotes that 7 of the 9 specimens used to measure the thickness change were subjected to mechanical testing.

Table 2

s-GAG content [μg/mg dry tissue weight] in the 4 quadrants and 3 experimental groups. Significant interaction between quadrant and group ($p < 0.0001$).

	ST	SN	IT	IN
Control	6.34 ± 1.91	8.62 ± 2.26	4.40 ± 1.19	4.49 ±1.11
Buffer-treated	7.54 ± 1.68	8.97 ± 2.61	4.93 ± 0.97	4.69 ± 1.01
Enzyme-treated	1.09 ± 0.23	0.90 ± 0.20	1.20 ± 0.25	1.18 ± 0.24

Table 3

Hydration ratio [mg/mg] in the 4 quadrants and 3 experimental groups. Nonsignificant interaction between quadrant and group ($p = 0.17$).

	ST	SN	IT	IN
Control	3.04 ± 0.066	3.15 ±0.093	3.04 ± 0.021	3.10 ± 0.063
Buffer-treated	3.26 ± 0.098	3.41 ±0.100	3.25 ± 0.055	3.26 ±0.100
Enzyme-treated	3.48 ± 0.080	3.52 ± 0.061	3.46 ±0.182	3.50± 0.174

Table 4

Thickness [mm] in the 4 quadrants and 3 experimental conditions. Non-significant interaction between quadrant and group ($p = 0.43$).

	ST	SN	IT	IN
Control	1.24 ± 0.145	1.10 ±0.071	0.95 ± 0.115	0.88 ± 0.121
Buffer-treated	1.32 ± 0.094	1.23 ±0.105	1.00 ±0.110	0.97 ±0.111
Enzyme-treated	1.32 ± 0.121	1.21 ±0.117	1.04 ± 0.114	1.04 ± 0.110

Table 5

Comparison of the mechanical outcomes, averaged over all quadrants, between the control and buffer-treated groups, in the circumferential and meridional directions. Paired Student's t-tests were used for statistical analysis.

	Circumferential			Meridional		
	Control	**Buffer-treated**	**p-value**	**Control**	**Buffer-treated**	**p-value**
Low-pressure stiffness [kPa]	496.3 ± 251.6	637.4 ± 348.1	<0.005	953.0 ± 724.8	1265.5 ± 1192.1	<0.05
High-pressure stiffness [kPa]	6747.3 ± 2045.9	5244.3 ± 1589.4	<0.0001	5595.2 ± 2604.4	4048.2 ± 1635.4	<0.005
Transition strain [mm/mm]	0.028 ± 0.012	0.027 ± 0.013	0.50	0.022 ±0.016	0.025 ± 0.020	0.16
Hysteresis [kPa]	0.18 ± 0.06	0.21 ± 0.08	<0.01	0.18 ±0.07	0.22 ± 0.10	<0.05
Initial creep rate (first 80 s) [s^{-1}]	0.033 ± 0.020	0.048 ± 0.021	<0.005	0.033 ±0.057	0.064 ± 0.078	0.11
Final creep rate (after 80 s) [s^{-1}]	0.062 ± 0.047	0.088 ± 0.040	<0.05	0.041 ± 0.058	0.16 ± 0.16	<0.005

Table 6

Comparison of the mechanical outcomes, averaged over all quadrants, between the buffer-treated and enzyme-treated groups, in the circumferential and meridional directions. Paired Student's t-tests were used for statistical analysis.

	Circumferential			**Meridional**		
	Buffer-treated	**Enzyme-treated**	**p-value**	**Buffer-treated**	**Enzyme-treated**	**p-value**
Low-pressure stiffness [kPa]	386.2 ± 206.7	187.2 ± 102.4	<0.0001	800.8 ± ± 759.5	364.7 ± 590.2	<0.0005
High-pressure stiffness [kPa]	3798.9 ± 1326.6	4673.5 ± 1677.6	<0.05	2881.1 ± 821.3	4477.1 ± 2131.0	<0.0005
Transition strain [mm/mm]	0.038 ±0.014	0.048 ± 0.017	0.001	0.034 ± 0.022	0.046 ± 0.026	<0.0005
Hysteresis [kPa]	0.27 ±0.10	0.20 ± 0.06	<0.0001	0.29 ±0.11	0.20 ± 0.08	<0.0001
Initial creep rate (first 80 s) [s^{-1}]	0.041 ± 0.020	0.037 ± 0.019	0.29	0.071 ± 0.079	0.030 ± 0.028	<0.001
Final creep rate (after 80 s) [s^{-1}]	0.11 ±0.12	0.096 ± 0.077	0.66	0.19 ± 0.25	0.11 ± 0.11	0.055

Table 7

Comparison of the mechanical outcomes, averaged over all quadrants, between the control and enzyme-treated groups, in the circumferential and meridional directions. Unpaired Student's t-tests were used for statistical analysis.

	Circumferential			Meridional		
	Control	Enzyme-treated	p-value	Control	Enzyme-treated	p-value
Low-pressure stiffness [kPa]	496.3 ± 251.6	187.2 ± 102.4	<0.0001	953.0 ± 724.8	364.7 ± 590.2	<0.005
High-pressure stiffness [kPa]	6747.3 ± 2045.9	4673.5 ± 1677.6	<0.0005	5595.2 ± 2604.4	4477.1 ± 2131.0	0.12
Transition strain [mm/mm]	0.028 ± 0.012	0.048 ±0.017	<0.0001	0.022 ± 0.016	0.046 ± 0.026	<0.001
Hysteresis [kPa]	0.18 ± 0.06	0.20 ± 0.06	0.31	0.18 ± 0.07	0.20 ± 0.08	0.47
Initial creep rate (first 80 s) [s^{-1}]	0.033 ± 0.020	0.037 ±0.019	0.47	0.033 ± 0.057	0.030 ± 0.028	0.86
Final creep rate (after 80 s) [s^{-1}]	0.062 ± 0.047	0.096 ±0.077	0.09	0.041 ± 0.058	0.11 ± 0.11	<0.05

Table 8

p-values for the comparison of the mechanical outcomes, averaged over all quadrants, between the circumferential and meridional directions, in the control, buffer-treated and enzyme-treated groups. Paired Student's t-tests were used for statistical analysis.

	Control	Buffer-treated	Enzyme-treated
Low-pressure stiffness	<0.005	<0.0001	0.09
High-pressure stiffness	0.13	<0.0001	0.65
Transition strain	<0.05	0.054	0.75
Hysteresis	0.60	0.55	0.79
Initial creep rate (first 80 s)	0.90	<0.05	0.24
Final creep rate (after 80 s)	0.39	0.001	0.59

Table 9

p-values for the interaction between group and quadrant for all mechanical outcomes. Linear mixed models were used for statistical analysis.

	Circumferential	Meridional
Low-pressure stiffness	0.01	<0.05
High-pressure stiffness	0.43	0.19
Transition strain	0.19	<0.005
Hysteresis	0.73	0.01
Initial creep rate (first 80 s)	0.20	0.09
Final creep rate (after 80 s)	0.99	0.92